Path entanglement of surface plasmons

2015 New J. Phys. 17 023002

(http://iopscience.iop.org/1367-2630/17/2/023002)

New Journal of Physics
The open access journal at the forefront of physics

Deutsche Physikalische Gesellschaft DPG
IOP Institute of Physics

Published in partnership with: Deutsche Physikalische Gesellschaft and the Institute of Physics

OPEN ACCESS

RECEIVED
22 October 2014

REVISED
16 December 2014

ACCEPTED FOR PUBLICATION
22 December 2014

PUBLISHED
30 January 2015

PAPER

Path entanglement of surface plasmons

James S Fakonas[1], **Anna Mitskovets**[1] **and Harry A Atwater**[1,2]

[1] Thomas J Watson Laboratories of Applied Physics, California Institute of Technology, Pasadena, CA 91125, USA
[2] Kavli Nanoscience Institute, California Institute of Technology, Pasadena, CA 91125, USA

E-mail: haa@caltech.edu

Keywords: plasmonics, quantum optics, path entanglement

Abstract

Metals can sustain traveling electromagnetic waves at their surfaces supported by the collective oscillations of their free electrons in unison. Remarkably, classical electromagnetism captures the essential physics of these 'surface plasma' waves using simple models with only macroscopic features, accounting for microscopic electron–electron and electron–phonon interactions with a single, semi-empirical damping parameter. Nevertheless, in quantum theory these microscopic interactions could be important, as any substantial environmental interactions could decohere quantum superpositions of surface plasmons, the quanta of these waves. Here we report a measurement of path entanglement between surface plasmons with 95% contrast, confirming that a path-entangled state can indeed survive without measurable decoherence. Our measurement suggests that elastic scattering mechanisms of the type that might cause pure dephasing in plasmonic systems must be weak enough not to significantly perturb the state of the metal under the experimental conditions we investigated.

Introduction

Classical models of surface plasma waves usually account for the microscopic scattering effects responsible for loss using a single, semi-empirical Drude damping parameter [1]. It is then straightforward to quantize these waves by analogy to electromagnetic fields in free space [2–5], with surface plasmons, their quanta, playing an analogous role to photons. Experiments in the last several years have tested this analogy, demonstrating single-particle statistics [6–9], squeezing [10], entanglement [11, 12], and quantum interference [13–17] in plasmonic circuits.

As hybrid excitations that involve both electromagnetic and electronic components, surface plasmons occupy an interesting middle ground between photonic systems, which typically interact weakly with their environments, and electronic systems, which usually suffer much stronger environmental interactions. In particular, classical theories of surface plasmons include extra microscopic interactions such as electron–electron, electron–phonon, and electron–surface scattering [1] that are absent for photons. These scattering mechanisms contribute both to the absorption of a plasmon, which creates an electron–hole pair, and the subsequent thermalization of the hot electron and hole. The full extent of these interactions is still a matter of some controversy, however, as elastic scattering processes might [18, 19] or might not [19, 20] cause 'pure dephasing' of plasmons that have not yet been absorbed.

If a surface plasmon scatters from phonons or electrons in the metal that supports it without being absorbed, thereby leaving behind a record of its existence in the electronic or atomic motions of the metal, it should be possible to detect such a scattering event as decoherence in a measurement of entanglement between plasmons. Experiments to date have shown that photons that are entangled by polarization [11] or frequency [12] do indeed remain entangled after being converted to plasmons and back to photons, but an experiment with path-entangled plasmons has not been reported. One reason the latter experiment is particularly interesting is that the entangled state should decohere if the metals involved (i.e. the 'environment') can detect the mere presence or absence of plasmons, as opposed to distinguishing between their polarization states or frequency components. We also note that the plasmonic waveguides we used for this experiment showed greater confinement,

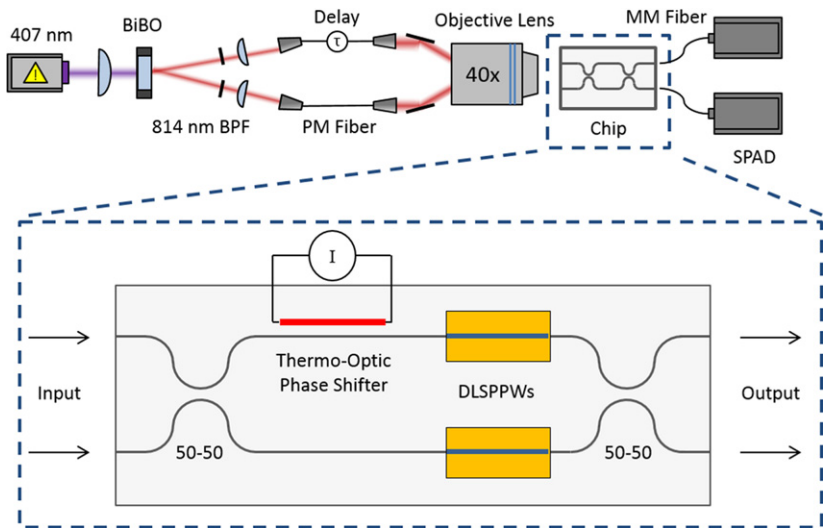

Figure 1. Schematic of path entanglement experiment. BiBO—bismuth borate crystal; BPF—band-pass filters (814 ± 2.5 nm); PM—polarization-maintaining; MM—multimode; SPAD—single-photon avalanche diode; DLSPPWs—dielectric-loaded surface plasmon polariton waveguides.

dispersion, and loss than those studied in previous entanglement experiments. Accordingly, we expect interactions between the plasmons and their environment to be stronger in our case.

Theory of experiment

Figure 1 shows a schematic of our experiment. We create pairs of single photons by spontaneous parametric down-conversion (SPDC) and couple them into a pair of waveguides which we fabricate on a silicon chip. The waveguides are coupled at two sequential 50–50 directional couplers, forming a Mach–Zehnder interferometer, and a resistive heater shifts the phase in one of the waveguides by the thermo-optic effect. Between the directional couplers, we integrate dielectrically loaded surface plasmon polariton waveguides (DSLPPWs) into the dielectric waveguides.

We used this circuit to study path-entanglement between surface plasmons as follows. Quantum interference at the first coupler produces a path-entangled state,

$$|1,1\rangle \otimes \left|E_i\right\rangle \xrightarrow{\text{1st coupler}} \frac{1}{\sqrt{2}}(|2,0\rangle + |0,2\rangle) \otimes \left|E_i\right\rangle, \tag{1}$$

where $|i,\ j\rangle$ denotes a state with i photons in one waveguide and j photons in the other, and $\left|E_i\right\rangle$ represents the state of the environment before the photons are converted to surface plasmons. Here, 'the environment' refers to all of the degrees of freedom of the electrons and phonons in the two metal pads that form the plasmonic waveguides. (We describe decoherence in this system using a von Neumann model of measurement, as described in section 3 of [21].) The heater introduces a phase shift to only the component in which both photons are in the first waveguide:

$$\frac{1}{\sqrt{2}}(|2,0\rangle + |0,2\rangle) \otimes \left|E_i\right\rangle \xrightarrow{\text{phase shift}} \frac{1}{\sqrt{2}}\left(e^{i2\Delta\phi}\,|2,0\rangle + |0,2\rangle\right) \otimes \left|E_i\right\rangle. \tag{2}$$

Note that the relative phase $\Delta\phi$ imparted by the heater contributes a phase to the state $|2,0\rangle$ which is twice as large. The factor of two comes from two powers of the creation operator, $a^\dagger$, each shifted by $\Delta\phi$, as in: $|2,0\rangle = \left(e^{i\Delta\phi}a^\dagger\right)^2 |0,0\rangle$.

At the plasmonic waveguides, the state of the environment evolves along with the state of the plasmons:

$$\frac{1}{\sqrt{2}}\left(e^{i2\Delta\phi}\,|2,0\rangle + |0,2\rangle\right) \otimes \left|E_i\right\rangle \xrightarrow{\text{plasmons}} \frac{1}{\sqrt{2}}\left(e^{i2\Delta\phi}\,|2,0\rangle \otimes \left|E_{2,0}\right\rangle + |0,2\rangle \otimes \left|E_{0,2}\right\rangle\right). \tag{3}$$

Here, $\left|E_{0,2}\right\rangle$ is the state of the environment that would result from both plasmons traversing the first waveguide, and $\left|E_{0,2}\right\rangle$ is the corresponding state for the other case. These two states are equal if the plasmons do not interact at all with their environment, but they would be different in the case that the plasmons elastically scatter from electrons or phonons, as described earlier. Note also that we have ignored components of the

resulting state that have fewer than two plasmons. Physically, this corresponds to post-selecting for only those trials in which neither plasmon was absorbed.

Finally, quantum interference at the second coupler produces a complicated output state:

$$\xrightarrow{\text{2nd coupler}} \frac{1}{4}\Big[e^{i2\Delta\phi}\Big(\sqrt{2}\ |2,0\rangle - 2i\ |1,1\rangle - \sqrt{2}\ |0,2\rangle\Big) \otimes \Big|E_{2,0}\Big\rangle + \Big(-\sqrt{2}\ |2,0\rangle - 2i\ |1,1\rangle + \sqrt{2}\ |0,2\rangle\Big) \otimes \Big|E_{0,2}\Big\rangle\Big]. \quad (4)$$

Constructing the density operator corresponding to this state and tracing over the degrees of freedom of the environment gives the reduced density operator of the surface plasmons, ρ_{red}, from which the probability of detecting simultaneous counts at the outputs can be found:

$$P_{\text{coinc}} = \langle 1,\ 1|\ \rho_{\text{red}}\ |1,\ 1\rangle = \frac{1}{2}\Big[\ 1 + \Big|\Big\langle E_{2,0}\ \Big|\ E_{0,2}\Big\rangle\Big|\ \cos(2\Delta\phi)\Big]. \quad (5)$$

In the absence of interactions between the plasmons and the environment, we have $\Big|E_{2,0}\Big\rangle = \Big|E_{0,2}\Big\rangle$ and, as a result, $P_{\text{coinc}} = \frac{1}{2}[1 + \cos(2\Delta\phi)]$. In contrast, if the surface plasmons alter the state of the metal such that $\Big|\Big\langle E_{2,0}\ \Big|E_{0,2}\Big\rangle\Big| < 1$, the amplitude of the sinusoidal oscillation of P_{coinc} is reduced, with the case $\Big|\Big\langle E_{2,0}\ \Big|E_{0,2}\Big\rangle\Big| = 0$ corresponding to total decoherence and no dependence of P_{coinc} on $\Delta\phi$. As a result, by measuring the coincidence count rate at the outputs of the waveguides as a function of the applied phase, $\Delta\phi$, we can probe the perseverance or decoherence of the path-entangled plasmon state.

Experimental methods

For our SPDC source, shown schematically in figure 1, we use a 100 mW, 407 nm diode laser and a bismuth borate (BiBO) crystal to generate pairs of single photons at 814 nm. Lenses on either side of the crystal focus the laser onto it and collect the divergent down-converted light from it. A pair of identical 5 nm band-pass filters centered at 814 nm isolate the down-converted photons from background light, and collimators collect them into polarization-maintaining fiber. When we connect these fibers to our silicon single photon avalanche diodes (SPADs), each roughly 50% efficient at this wavelength, we observe approximately 26 000 coincidence counts per second.

The waveguide-coupling apparatus, also depicted in figure 1, consists of a 40× microscope objective that focuses the photons into the input side of the chip, lensed multimode fibers to collect them from the output side of the chip, and SPADs to detect them. We use a fiber-coupled adjustable delay line to ensure that both photons arrive at the chip simultaneously, which we verify by observing Hong–Ou–Mandel interference [24] as we vary the delay setting. We observe approximately 6% transmission through a circuit with 10 μm DLSPPWs and 3% transmission through one with 20 μm DLSPPWs.

We fabricate our interferometers on silicon chips using a combination of lithography, wet and dry etching, and thin film deposition techniques, which are described in more detail in [14]. Briefly, we pattern the dielectric waveguides in 280 nm of silicon nitride on top of a 3 μm SiO_2 lower cladding layer. Subsequent lithography, etching, deposition, and lift-off steps define recessed gold pads for the DLSPPWs, followed by further lithography and metallization steps to create nickel-chromium heaters and gold contact pads. Two final lithography steps in 2.5 μm and 350 nm PMMA cover layers define spot-size converters [23] at the ends of the waveguides and the dielectric loads of the DSLPPWs, respectively. The completed DLSPPWs consist of strips of PMMA 300 nm wide, 350 nm tall, and either 10 or 20 μm long on top of gold pads of the same length.

Figure 2 shows the fabricated chip. Panel (a) depicts two complete interferometers, each with a pair of contact pads (large gold rectangles) and 10 μm DLSPPWs (small gold rectangles, shown also in panel (c)). The large, dark oval near the center of the image is an area where the silicon underneath the waveguides has been etched away using XeF_2 in order to thermally isolate the resistive heaters, which can be seen more clearly in panel (b). The diagram in panel (d) sketches a cross section of this part of the chip, showing the heater-waveguide separation and the approximate extent of the undercut. With this design, we need roughly 50 times less power to achieve a given phase shift than for a similar chip without the undercut.

The measurements themselves consist of two main steps. First, we set the heater power to give a phase shift of approximately $\pi/2$ and record simultaneous counts at the detectors as a function of the adjustable delay setting. The resulting Hong–Ou–Mandel interference allows us to find the setting that corresponds to the simultaneous arrival of both photons at the first directional coupler. Second, we step the voltage across the heater from 0–3 V (roughly 0–5 mW), recording both one- and two-particle interference in the count rates of the SPADs. Specifically, at each step we: (1) block one of the inputs and record the count rate on each detector; (2) unblock

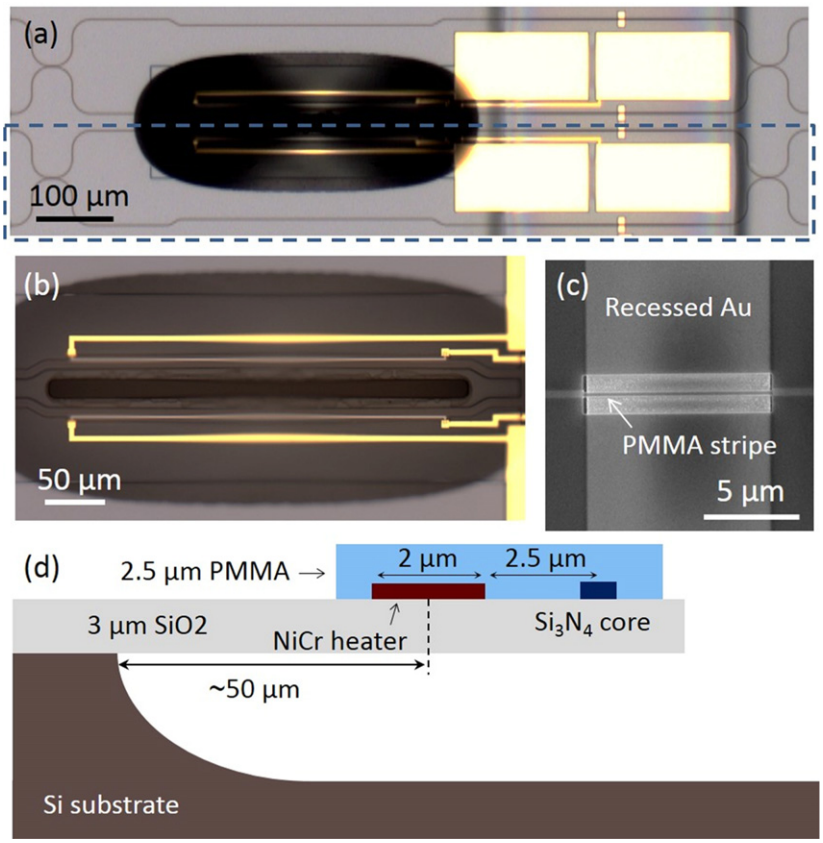

Figure 2. The completed chip. (a) Optical micrograph showing dielectric waveguides (thin dark lines), contact pads (large gold rectangles), DLSPPWs (small gold rectangles), and under-etched region (large dark oval). The two dark, vertical lines in the right half of the image separate the area covered with 350 nm of PMMA (between these lines) from that covered with 2.5 μm of PMMA (everywhere else). The dashed box encloses a single interferometer with 10 μm DLSPPWs, as represented schematically in figure 1. (b) Optical micrograph of the region where the silicon handle has been etched out from underneath the heaters and waveguides. The two light gray, horizontal lines connecting pairs of gold contacts are resistive NiCr heaters, while the long, dark oval between them is the hole through which the underlying silicon was etched. (c) Scanning electron micrograph of a 10 μm DLSPPW. (d) Diagram showing a cross section of the under-etched region.

the input and record the coincidence count rate; and (3) block the same input as before and record the separate count rates again to make sure they did not change substantially. Following this procedure allows us to observe single-particle ('classical') interference in the data with one input blocked and two-particle interference in the coincidence data.

Results and conclusions

Our raw data for the 10 μm DLSPPWs are shown in figure 3(a). The top panel shows the count rate of one of the SPADs with one input blocked (i.e. one-particle interference), while the bottom panel shows the coincidence count rate with neither input blocked. Both signals oscillate, and it is clear that the latter does so at twice the frequency of the former. The oscillations are not sinusoidal, though, indicating that the phase shift caused by the heater does not depend linearly on the power supplied to it. We also note that the heater itself was quite stable, as its resistance, shown in figure 3(b), did not change by more than about 1% over the course of the measurement. Taking the thermo-optic coefficient of the silicon nitride to be 2.45e–5 [22] and neglecting the contributions of the cladding materials, we estimate that the heaters increase the temperature of the neighboring waveguides by about 70 °C.

From the single-particle interference in the top panel of figure 3(a), we calculate the phase shift that the heater produced at each power setting. The result is shown in figure 3(c). We then use this information to plot the coincidence data as a function of phase instead of heater power, as shown in figure 4(a). The data in this plot are the same as those in the bottom panel of figure 3(a), but here they are plotted as a function of the phase shift induced by the heater. The red curve shows a sinusoidal fit with a period of π, confirming that the coincidence signal does indeed oscillate as expected from equation (5). Figure 4(b) shows the result of a similar measurement made in an interferometer with 20 μm DLSPPWs, where we have applied the same method of analysis. The

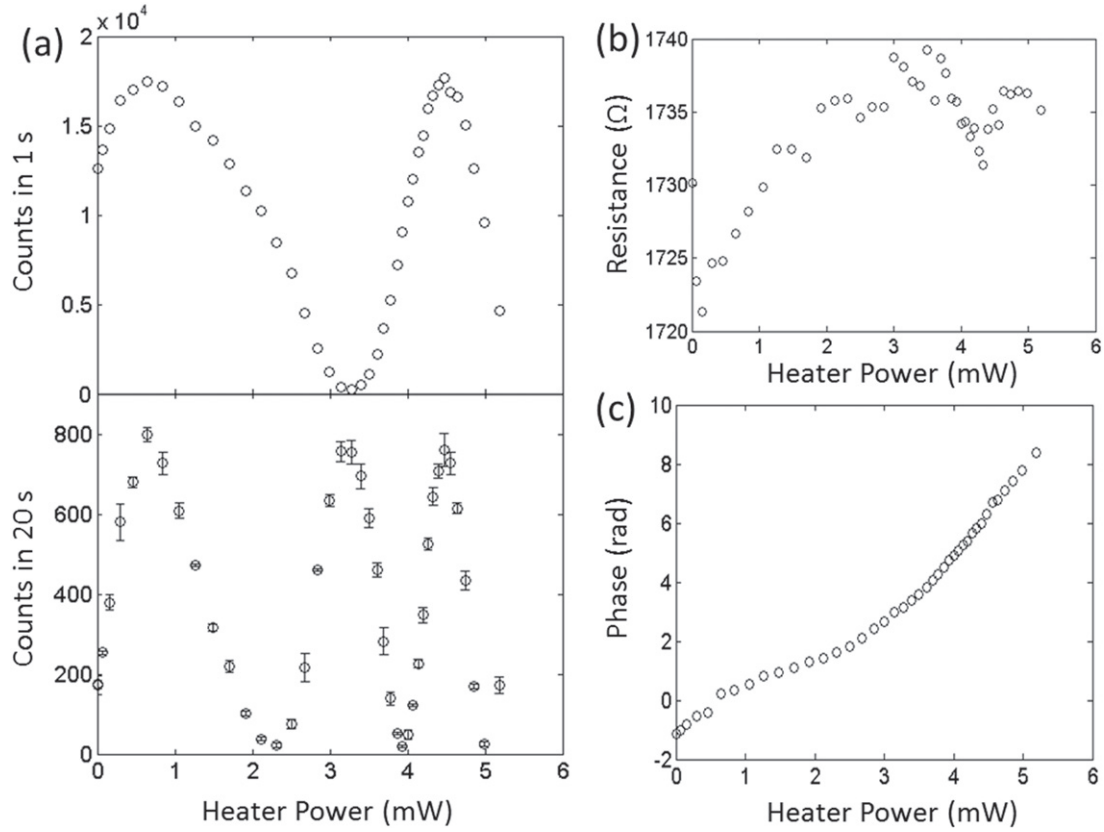

Figure 3. Raw measurements on the interferometer that had 10 μm DLSPPWs. (a) Top: one-particle interference obtained by blocking one input of the interferometer and recording the count rate at one of the detectors. Bottom: two-particle interference obtained by counting coincidences with both inputs unblocked. Error bars indicate one sample standard deviation above and below the average, calculated from three trials. (b) Resistance of the NiCr heater plotted over its operating range, showing a maximum variation of about 1%. (c) Plot of the phase shift induced by the heater as a function of the power supplied to it, computed from the one-particle interference data. The first maximum of the interference data was taken to correspond to zero phase.

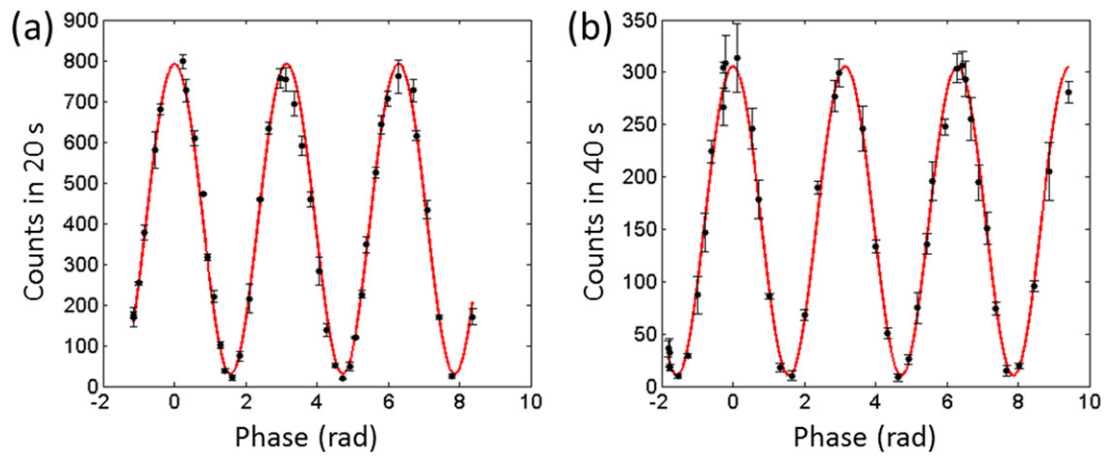

Figure 4. Measurements of two-particle interference in the interferometers with 10 μm (left) and 20 μm (right) DLSPPWs showing clear path entanglement with visibilities of 0.954 ± 0.016 and 0.948 ± 0.021, respectively. Each data point marks the average of three measurements, while the error bars represent one sample standard deviation above and below the average. The red curves are sinusoidal fits.

result is nearly identical to that in panel (a), indicating that increasing the length of the DLSPPWs (and therefore the losses suffered) did not affect the degree of path entanglement.

The visibility of interference in these measurements is defined as

$$V = \frac{C_{\max} - C_{\min}}{C_{\max} + C_{\min}} = 1 - \frac{2C_{\min}}{C_{\max} + C_{\min}}, \quad (6)$$

where $C_{\max}$ and $C_{\min}$ are the maximum and minimum count rates observed as the phase varies. In the interferometer with 10 μm DLSPPWs we observe one-particle and two-particle interference with visibilities of 0.974 ± 0.005 and 0.954 ± 0.016, respectively. In each of these calculations, we estimate the standard deviation of the visibility using the (measured) standard deviation of $C_{\min}$, taking $C_{\max}$ to be constant because fluctuations in $C_{\max}$ are proportionately much smaller than fluctuations in $C_{\min}$. In the circuit with 20 μm DLSPPWs, we observe visibilities of 0.972 ± 0.007 and 0.948 ± 0.021 for one- and two-particle interference, respectively.

While the longer, higher-loss waveguides did not reduce the visibility of entanglement, they certainly reduced the overall transmission of light through the interferometers. As shown in figure 4, increasing the length of the DLSPPWs by 10 μm reduced the coincidence count rate by roughly a factor of five, which is consistent with the observed drop in the single-particle signal by slightly more than a factor of two. In previous measurements [14], we estimated the $1/e$ absorption length in similar waveguides to be roughly 7 μm, however, which suggests that the difference between losses observed in the 10 μm and 20 μm waveguides in the current experiment should have been larger. We suspect that the coupling of light into and out of the interferometer with 20 μm DLSPPWs might have been slightly more efficient than for the interferometer with 10 μm DLSPPWs, partially offsetting the extra absorption loss.

In conclusion, we have observed path entanglement between surface plasmons with a visibility of approximately 95%. Moreover, doubling the length of the plasmonic waveguides we studied did not have any measurable effect on the visibility of entanglement. As a result, we conclude that the plasmons in our experiment did not interact strongly enough with the metal that sustained them—as by elastically scattering electrons or phonons, for example—to decohere the path-entangled state.

Acknowledgments

This work was supported by the Air Force Office of Scientific Research under MURI Awards FA9550-12-1-0488 (JSF) and FA9550-12-1-0024 (AM). Additionally, we gratefully acknowledge the Kavli Nanoscience Institute at Caltech for access to and maintenance of fabrication equipment.

References

[1] Liu M, Pelton M and Guyot-Sionnest P 2009 Reduced damping of surface plasmons at low temperatures *Phys. Rev.* B **79** 035418
[2] Elson J M and Ritchie R H 1971 Photon interactions at a rough metal surface *Phys. Rev.* B **4** 4129–38
[3] Tame M S, Lee C, Lee J, Ballester D, Paternostro M, Zayats A V and Kim M S 2008 Single-photon excitation of surface plasmon polaritons *Phys. Rev. Lett.* **101** 190504
[4] Archambault A, Marquier F, Greffet J-J and Arnold C 2010 Quantum theory of spontaneous and stimulated emission of surface plasmons *Phys. Rev.* B **82** 035411
[5] Tame M S, McEnery K R, Ozdemir S K, Lee J, Maier S A and Kim M S 2013 Quantum plasmonics *Nat. Phys.* **9** 329–40
[6] Akimov A V, Mukherjee A, Yu C L, Chang D E, Zibrov A S, Hemmer P R, Park H and Lukin M D 2007 Generation of single optical plasmons in metallic nanowires coupled to quantum dots *Nature* **450** 402–6
[7] Kolesov R, Grotz B, Balasubramanian G, Stohr R J, Nicolet A A L, Hemmer P R, Jelezko F and Wrachtrup J 2009 Wave-particle duality of single surface plasmon polaritons *Nat. Phys.* **5** 470–4
[8] Heeres R W, Dorenbos S N, Koene B, Solomon G S, Kouwenhoven L P and Zwiller V 2010 On-chip single plasmon detection *Nano Lett.* **10** 661–4
[9] Di Martino G, Sonnefraud Y, Kena-Cohen S, Tame M, Ozdemir S K, Kim M S and Maier S A 2012 Quantum statistics of surface plasmon polaritons in metallic stripe waveguides *Nano Lett.* **12** 2504–8
[10] Huck A, Smolka S, Lodahl P, Sorensen A S, Boltasseva A, Janousek J and Andersen U L 2009 Demonstration of quadrature-squeezed surface plasmons in a gold waveguide *Phys. Rev. Lett.* **102** 246802
[11] Altewischer E, van Exter M P and Woerdman J P 2002 Plasmon-assisted transmission of entangled photons *Nature* **418** 304–6
[12] Fasel S, Robin F, Moreno E, Erni D, Gisin N and Zbinden H 2005 Energy-time entanglement preservation in plasmon-assisted light transmission *Phys. Rev. Lett.* **94** 110501
[13] Heeres R W, Kouwenhoven L P and Zwiller V 2013 Quantum interference in plasmonic circuits *Nat. Nanotechnology* **8** 719–22
[14] Fakonas J S, Lee H, Kelatia Y A and Atwater H A 2014 Two-plasmon quantum interference *Nat. Photonics* **8** 317–20
[15] Di Martino G, Sonnefraud Y, Tame M S, Kena-Cohen S, Dieleman F, Ozdemir K, Kim M S and Maier S A 2014 Observation of quantum interference in the plasmonic Hong–Ou–Mandel effect *Phys. Rev. Appl.* **1** 034004
[16] Fujii G, Fukuda D and Inoue S 2014 Direct observation of bosonic quantum interference of surface plasmon polaritons using photon-number-resolving detectors *Phys. Rev.* B **90** 085430
[17] Cai Y-J, Li M, Ren X-F, Zou C-L, Xiong X, Lei H-L, Liu B-H, Guo G-P and Guo G-C 2014 High-visibility on-chip quantum interference of single surface plasmons *Phys. Rev. Appl.* **2** 014004

[18] Guo Z, Habenicht B F, Liang W-Z and Prezhdo O V 2010 Ab initio study of phonon-induced dephasing of plasmon excitations in silver quantum dots *Phys. Rev.* B **81** 125415
[19] Scharte M, Porath R, Ohms T, Aeschlimann M, Lamprecht B, Ditlbacher H and Aussenegg F R 2001 Lifetime and dephasing of plasmons in Ag nanoparticles *Proc. SPIE* **4456** 14
[20] Sonnichsen C, Franzl T, Wilk T, von Plessen G and Feldmann J 2002 Drastic reduction of plasmon damping in gold nanorods *Phys. Rev. Lett.* **88** 077402
[21] Schlosshauer M 2004 Decoherence, the measurement problem, and interpretations of quantum mechanics *Rev. Mod. Phys.* **76** 1267–305
[22] Arbabi A and Goddard L L 2013 Measurements of the refractive indices and thermo-optic coefficients of Si_3N_4 and SiO_x using microring resonances *Opt. Lett.* **38** 3878–81
[23] Shoji T, Tsuchizawa T, Watanabe T, Yamada K and Morita H 2002 Low loss mode size converter from 0.3 μm square si wire waveguides to singlemode fibres *Electron. Lett.* **38** 1669–70
[24] Hong C K, Ou Z Y and Mandel L 1987 Measurement of subpicosecond time intervals between two photons by interference *Phys. Rev. Lett.* **59** 2044–6